1-1-2014

Dynamical (e,2e) Studies of Tetrahydropyran and 1,4-Dioxane

J. D. Builth-Williams

G. Da Silva

L. Chiari

D. B. Jones

et. al. For a complete list of authors, see https://scholarsmine.mst.edu/phys_facwork/448

Recommended Citation

J. D. Builth-Williams et al., "Dynamical (e,2e) Studies of Tetrahydropyran and 1,4-Dioxane," *Journal of Chemical Physics*, vol. 140, no. 21, American Institute of Physics (AIP), Jan 2014.
The definitive version is available at https://doi.org/10.1063/1.4880204

Dynamical (e,2e) studies of tetrahydropyran and 1,4-dioxane

J. D. Builth-Williams,[1] G. B. da Silva,[1,2] L. Chiari,[1] D. B. Jones,[1,a)] Hari Chaluvadi,[3] D. H. Madison,[3] and M. J. Brunger[1,4,a)]
[1]*School of Chemical and Physical Sciences, Flinders University, GPO Box 2100, Adelaide, South Australia 5001, Australia*
[2]*Universidade Federal de Mato Grosso, Barra do Garças, MT 78600-000, Brazil*
[3]*Department of Physics, Missouri University of Science and Technology, Rolla, Missouri 65409, USA*
[4]*Institute of Mathematical Sciences, University of Malaya, 50603 Kuala Lumpur, Malaysia*

(Received 8 April 2014; accepted 16 May 2014; published online 4 June 2014)

We present experimental and theoretical results for the electron-impact ionization of the highest occupied molecular orbitals of tetrahydropyran and 1,4-dioxane. Using an (e,2e) technique in asymmetric coplanar kinematics, angular distributions of the slow ejected electron, with an energy of 20 eV, are measured when incident electrons at 250 eV ionize the target and scatter through an angle of either -10° or -15°. The data are compared with calculations performed at the molecular 3-body distorted wave level. Fair agreement between the theoretical model and the experimental measurements was observed. The similar structures for these targets provide key insights for assessing the limitations of the theoretical calculations. This study in turn facilitates an improved understanding of the dynamics in the ionization process. © *2014 AIP Publishing LLC*. [http://dx.doi.org/10.1063/1.4880204]

I. INTRODUCTION

The interaction between low-energy charged particles with molecules of biological significance has attracted great interest in the last decade. In some medical procedures, such as radiotherapy and medical imaging, living tissue is routinely exposed to ionizing radiation. Here, a single high-energy ionizing particle can induce a cascade of ionization events that can produce up to 3×10^4 low-energy secondary electrons.[1] These low energy electrons may then cause cell damage or death by initiating mutagenic, genotoxic or DNA lesions.[2] In this respect, low-energy electrons are probably the most important species in radiation chemistry.[3] In order to predict the effects of exposing living tissue to ionizing radiation, many groups have developed Monte Carlo track structure codes[4–11] that simulate the charged-particle paths. However, the majority of these track simulations have been formulated assuming that the biological medium consists entirely of water. This practice probably reflects the lack of available data for complex biomolecules that can be included in the Monte Carlo codes. Here the absence of robust molecular scattering data sets reflects the inherent difficulty in performing experimental measurements and computationally demanding theoretical calculations for studying complex biomolecules.

In this context, there have been recent systematic investigations to study the dynamics of the ionization processes for molecules that can approximate the building blocks of a biological system. These have included water,[12] DNA bases and their sub-structures (pyrimidine,[13] thymine[14]) and analogues to the DNA backbone (tetrahydrofuran[15,16] and tetrahydrofuryl alcohol[16,17]). To utilize these measurements in Monte Carlo simulations, complete cross section sets over a wide range of projectile energies and kinematical conditions are required. It has become apparent that the long experimental run times required for obtaining triple differential cross sections limits the capability of experiments to measure complete cross section sets over the large range of incident electron energies and the kinematical conditions that are required for Monte Carlo based simulation codes. This generates an urgent demand for developing theoretical models that can reliably and efficiently generate such complete cross section sets. It is therefore important that experimental measurements provide a strong foundation for assessing the importance of chemical composition and structure on the electron scattering behavior, so that theoretical computations can be benchmarked, and their limitations established, over a range of kinematical conditions.

We have previously investigated electron-impact ionization of the structurally similar cyclic ethers tetrahydrofuran (THF),[15] tetrahydropyran (THP),[15] and 1,4-dioxane,[15] with kinematical conditions that investigated the Bethe surface well-below the bound Bethe Ridge.[15] Here we expand that work with additional experimental measurements and calculations for the ionization of the highest occupied molecular orbitals (HOMOs) of both THP ($15a'$ orbital) and 1,4-dioxane ($8a_g$ orbital). For both targets the HOMO is dominated by the out-of plane Oxygen ($2p$) contribution. The similar, yet different, structures of these targets provide opportunities to gain insights into the importance of structure in the dynamics of ionization. By combining these measurements with our earlier data[15] we can map the Bethe surface for these species below the bound Bethe ridge. The investigation of ionization dynamics for kinematical conditions that map the Bethe surface, below the bound Bethe ridge, are essential for understanding the dynamics of the electron-impact ionization process. Here the experimental results are compared to theoretical calculations obtained within a molecular 3-body distorted

a)Authors to whom correspondence should be addressed: Electronic addresses: darryl.jones@flinders.edu.au and michael.brunger@flinders.edu.au

wave (M3DW) framework. Through the comparison of theory and experimental data over structurally similar targets it is becoming feasible to fully assess the limitations of theoretical models and identify how they may be improved.

II. EXPERIMENTAL METHOD

We have used an (e,2e) coincidence technique under asymmetric coplanar kinematical conditions, in order to obtain triple differential cross sections for electron-impact ionization of THP and 1,4-dioxane. The full details of the method employed can be found in Refs. 15, 18, and 19. Briefly, a highly collimated beam of electrons with well-defined energy E_0 and momentum $\boldsymbol{p}_0$, is incident on a beam of the target molecule, M. When the target is ionized, the fast (scattered) and slow (ejected) electrons are detected. Here a time-coincidence method is used to ensure that the two detected electrons originated from the same ionization event. The kinematically complete reaction can be described by

$$e_0^-(E_0, \boldsymbol{p}_0) + M \rightarrow M^+(\epsilon_i, \boldsymbol{q}) + e_a^-(E_a, \boldsymbol{p}_a) + e_b^-(E_b, \boldsymbol{p}_b), \tag{1}$$

where M^+ is the residual ion produced in the ionization process. The energies and momenta for the scattered and ejected electrons are given by $(E_a, \boldsymbol{p}_a)$ and $(E_b, \boldsymbol{p}_b)$, respectively. ϵ_i is the energy required to ionize the ith molecular orbital. The conservation of energy during the ionization process requires

$$E_0 = \epsilon_i + E_a + E_b. \tag{2}$$

Likewise, to conserve linear momentum during the ionization process, the residual ion recoils with momentum:

$$\boldsymbol{q} = \boldsymbol{p}_0 - (\boldsymbol{p}_a + \boldsymbol{p}_b). \tag{3}$$

In the present asymmetric kinematics, the incident electron and slow electron energies are fixed at $E_0 = 250$ eV and $E_b = 20$ eV, respectively. Angular distributions of the slow ejected electron (θ_b) are measured while the direction of the fast electron is fixed at polar angles of either $\theta_a = -10^\circ$ or -15°. Note that all angles are referenced to the incident electron beam direction. The angle through which the incident electron is deflected also defines the momentum transferred to the target:

$$\boldsymbol{K} = \boldsymbol{p}_0 - \boldsymbol{p}_a. \tag{4}$$

The ionization potentials of the HOMO's of THP (15a′ orbital) and 1,4-dioxane ($8a_g$ orbital) are 9.46 and 9.37 eV,[20] respectively. When the scattered electron is detected at $\theta_a = -10^\circ$ or -15° the magnitudes of the momentum transfer are 0.77 and 1.12 a.u., respectively. For an ejected electron with $E_b = 20$ eV ($|\boldsymbol{p}_b| = 1.21$ a.u.), these momentum values lie below and approximate the bound Bethe-Ridge condition of $|\boldsymbol{K}| = |\boldsymbol{p}_b|$. These measurements can be combined with earlier measurements at $\theta_a = -5^\circ$ ($|\boldsymbol{K}| = 0.45$ a.u.) to map out the ionization behavior below the bound Bethe-Ridge. Under these conditions the magnitude of the momentum transfer and the ejected electron's momentum are comparable to the momentum of the valence electrons bound to the target.

When the ejected electron leaves the collision in a direction close to that of the momentum transfer ($+\boldsymbol{K}$), the recoil momentum is minimized, and the collisions are said to be binary. Similarly, when the electron is ejected in a direction nearly anti-parallel to that of the momentum transfer ($-\boldsymbol{K}$), the target recoil momentum must be at its maximum to conserve momentum. In this angular region, collisions are said to be recoil in nature.

III. THEORETICAL METHOD

Within the molecular 3-body distorted wave (M3DW) framework, the electron-impact ionization scattering amplitude can be described by

$$T = \left\langle \chi_a^-(\boldsymbol{k}_a, \boldsymbol{r}_1)\, \chi_b^-(\boldsymbol{k}_b, \boldsymbol{r}_2)\, C_{scat-ejec}\left(r_{12}^{ave}\right) \middle| V - U_0 \middle| \phi_{DY}^{OA}(\boldsymbol{r}_2) \chi_0^+(\boldsymbol{k}_0, \boldsymbol{r}_1) \right\rangle. \tag{5}$$

Here the initial state is described as the product of an incident distorted wave $\chi_0^+(\boldsymbol{k}_0, \boldsymbol{r}_1)$ and the orientation averaged Dyson orbital $\phi_{DY}^{OA}(\boldsymbol{r}_2)$. Within a frozen orbital approximation, the Dyson orbital is described by the ionized Kohn-Sham orbital of the target ground state. In this work, the molecular wave functions were calculated using density functional theory (DFT) along with the standard hybrid B3LYP[21] functional using the ADF 2007 (Amsterdam Density Functional) program[22] with the TZ2P (triple-zeta with two polarization functions) Slater type basis set. The final state was described by distorted waves $\chi_a^-(\boldsymbol{k}_a, \boldsymbol{r}_1)$ and $\chi_b^-(\boldsymbol{k}_b, \boldsymbol{r}_2)$ for the fast and slow outgoing electrons, and the Ward-Macek[23] Coulomb distortion factor, $C_{scat-ejec}(r_{12}^{ave})$. The initial interaction between the incident electron and the neutral molecule is described by the potential V, while U_0 is a spherically symmetric distorting potential which is used to calculate the incident initial-state distorted wave, $\chi_0^+(\boldsymbol{k}_0, \boldsymbol{r}_1)$. Here the distorted waves are calculated using a distorting potential that combines the exchange potential of Furness and McCarthy (corrected for sign errors),[24] the correlation potential of Perdew and Zunger[25] (see also Padial and Norcross[26]) and a spherically symmetric target potential that combines the target electron charge density (obtained by summing $2|\phi_j(\boldsymbol{r})|^2$ over all occupied orbitals) and spheres that describe the different charged nuclei within the center-of-mass frame. The parameters describing the distorting potential of THP and 1,4-dioxane are the same as those employed previously.[15] The final state distorted waves are obtained in the same way except that the potential U_0 is modified to account for the change in the final state charge density.

The triple differential cross section for electron-impact ionization can be obtained through:

$$\frac{d\sigma}{d\Omega_a d\Omega_b dE_b} = \frac{1}{(2\pi)^5} \frac{k_a k_b}{k_0} (|T_{dir}|^2 + |T_{exc}|^2 + |T_{dir} - T_{exc}|^2). \tag{6}$$

Here T_{dir} and T_{exc} are the direct and exchange scattering amplitudes, respectively. Both amplitudes are calculated using Eq. (5) with and without the interchange of the electrons in

the final state. The full description of this theoretical method can be obtained in Refs. 16, 27–29.

IV. RESULTS

In Figures 1 and 2, the experimental TDCS for electron-impact ionization of the highest occupied molecular orbital (HOMO) of THP (15a′ orbital) and 1,4-dioxane ($8a_g$ orbital), respectively, are presented when the scattered electron is detected at (a) $\theta_a = -5°$,[15] (b) $\theta_a = -10°$, and $\theta_a = -15°$. Note that a small error that affected the binary recoil ratio was found in our previous experimental analysis.[15] The corrected experimental data for $\theta_a = -5°$ are presented here. Also shown in these figures are the theoretical TDCSs obtained within the M3DW method, to compare with the experimental measurements. Here the experimental data have been normalized to the M3DW calculation in order to obtain the best visual fit in the binary region. We begin by first comparing the experimental data to the theoretical calculations for each molecule independently. This is then followed by a discussion about how the respective structures of the molecules may influence the observed scattering dynamics and how these results may improve our understanding of the ionization process.

A. Tetrahydropyran (THP)

For the measurements at $\theta_a = -10°$, the intensity observed in the binary region is quite broad, having significant intensity over the measured angular range of the experiment. This observation is consistent with the wide binary peak calculated within the M3DW model. The M3DW calculation predicts a large peak centered close to the momentum transfer direction that has a significant shoulder close to $\theta_b \sim 90°$. While this peak structure is not observed in the experimental data for $\theta_a = -10°$, the experiment exhibits the shoulder structure predicted by the theory. In the recoil region for $\theta_a = -10°$, the experimental data certainly suggest that a peak may exist in the angular region of $\theta_b \sim 270°$. While the M3DW does predict a number of small peaks at different angular positions, the intensity of these features is significantly below that which is observed experimentally.

For THP at a scattering angle of $\theta_a = -15°$, the experimental data in the binary region suggest two experimental features. Here there is a peak observed in the direction of the momentum transfer that has a substantial shoulder in the $\theta_b \sim 90°$–$120°$ angular range. The M3DW calculation also predicts the peak and shoulder in the binary region. However, the calculation does underestimate the intensity of the shoulder. In the recoil region, the experimental data again suggest the presence of a peak that has been shifted away from the direction anti-parallel to the momentum transfer. However, the finite angular range of our experimental measurements, limited by the physical constraints of the detectors, limits the full assessment of the shape of this feature. Note that the M3DW does predict a relatively substantial peak, compared to that at $\theta_a = -10°$, in the recoil region. This feature is, however,

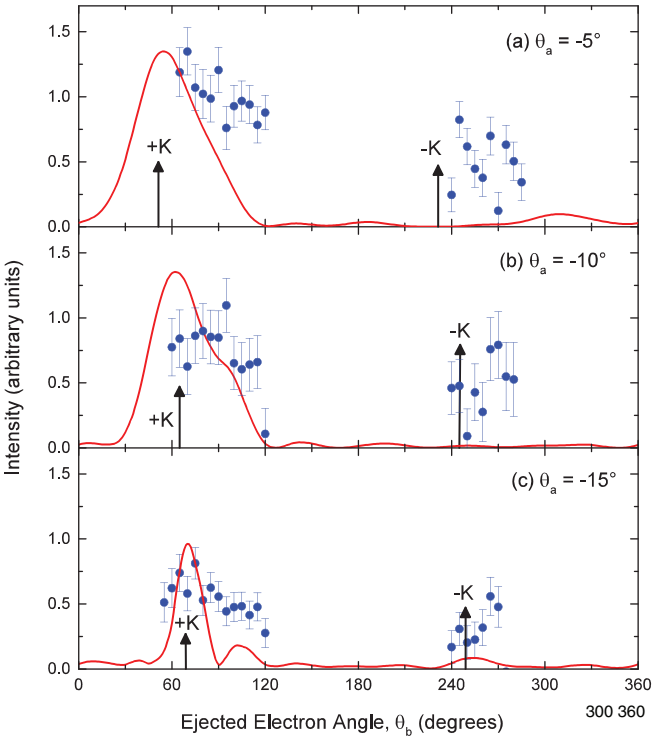

FIG. 1. TDCS for electron impact ionization of the HOMO of THP (15a′) with $E_0 = 250$ eV, $E_b = 20$ eV and transferred momentum (a) K = 0.45 a.u. ($\theta_a = -5°$), (b) K = 0.77 a.u. ($\theta_a = -10°$), and (c) K = 1.12 a.u. ($\theta_a = -15°$). The M3DW calculation results (——) are compared to the experimental data (●). The directions parallel (+K) and anti-parallel (−K) to the transferred momentum are represented by the arrows.

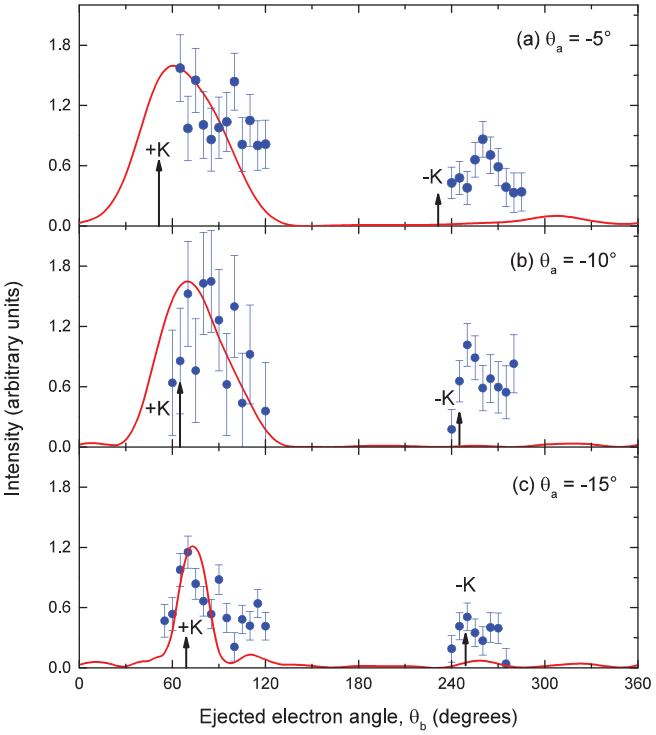

FIG. 2. TDCS for electron impact ionization of the HOMO of 1,4-dioxane ($8a_g$) with $E_0 = 250$ eV, $E_b = 20$ eV and momentum transfer values of (a) K = 0.45 a.u. ($\theta_a = -5°$), (b) K = 0.77 a.u. ($\theta_a = -10°$), and (c) K = 1.12 a.u. ($\theta_a = -15°$). Experimentally measured data (●) and M3DW calculation results (——) are plotted. The directions parallel (+K) and anti-parallel (−K) to the transferred momentum are represented by the arrows.

centered in the direction anti-parallel to the momentum transfer. The intensity of this feature is also below that observed experimentally.

B. 1,4-Dioxane

The experimental data for 1,4-dioxane at $\theta_a = -10^\circ$ display a broad peak in the binary region. This peak has been shifted away from the momentum transfer direction and has a maximum at $\theta_b \sim 80^\circ$. The M3DW calculation also predicts a single broad peak in the binary region under this kinematical condition. Both the experimental data and the M3DW calculations display asymmetry in the peak profile, which has a significant tail in the 90°–120° angular range. While the M3DW predicts the correct shape for this binary feature, it appears to overestimate the width observed experimentally. Also, the M3DW underestimates the shift of this peak away from the momentum transfer direction.

At $\theta_a = -15^\circ$, the experimental data for 1,4-dioxane contain two spectral features in the binary region; it has a strong peak located along the momentum transfer direction, and a shoulder in the $\theta_b \sim 90^\circ$–120° angular range. For $\theta_a = -15^\circ$, the M3DW calculation does a good job at reproducing the shape of the TDCS in the binary region, although again in this case, the M3DW calculation fails to predict the substantial intensity observed experimentally for the shoulder. In the recoil region, the M3DW predicts a peak close to the direction anti-parallel to the momentum transfer. This peak position is consistent with that of the experimental data observed in this recoil region. However, the intensity of this recoil peak predicted by the M3DW calculation still significantly underestimates the magnitude of the experimental data.

C. Discussion

Owing to the structural similarities between THP and 1,4 dioxane, it is interesting to establish how these structures influence the cross sections. In this way we hope to provide a foundation for understanding the importance of structure in the dynamics of the ionization process. To assist in this discussion, the M3DW calculations for THP and 1,4-dioxane are compared in Fig. 3.

From Fig. 3, it is apparent that the TDCS for both THP and 1,4-dioxane have a number of similar features in the calculated cross sections at the M3DW level. Here the peak positions of the binary and recoil features are in good accord across the two different targets. In the cross sections for all scattering angles there are a number of peaks and troughs at the intermediate angles between the binary and recoil features. The positioning of these features, and their relative shifts as the kinematical conditions change, reveal that these features are related to the similar structures of the targets. Specifically, the presence of these minima appears to reflect an interference-like effect. It is interesting to note that minima in 1,4 dioxane are more prominent than those observed in THP. Here the higher symmetry of 1,4-dioxane places all of the nuclear charge on 4-nuclear spheres that may make nuclear interference effects much more prominent. For THP, the

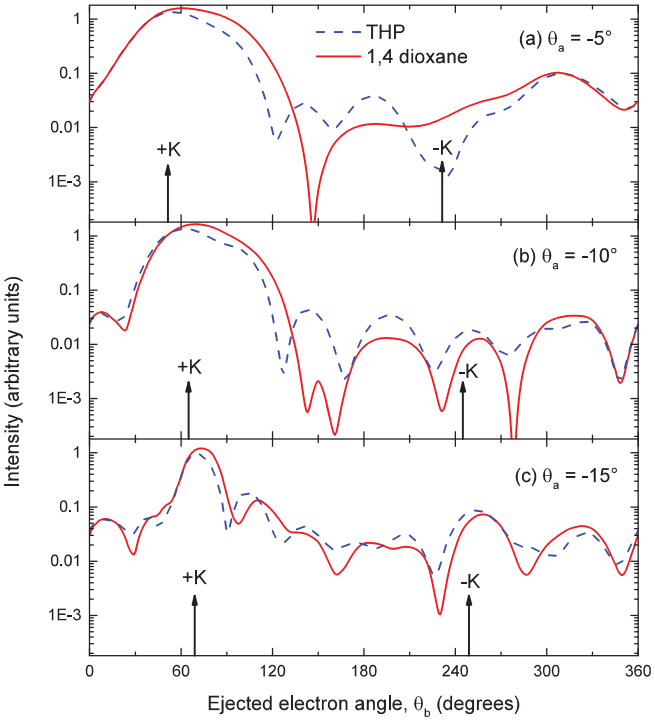

FIG. 3. Comparison of the M3DW TDCS for the 15a′ HOMO of THP (— —) and the $8a_g$ HOMO of 1,4-dioxane (——), calculated for E_0 = 250 eV, E_b = 20 eV and momentum transfer values of (a) K = 0.45 a.u. ($\theta_a = -5^\circ$), (b) K = 0.77 a.u. ($\theta_a = -10^\circ$), and (c) K = 1.12 a.u. ($\theta_a = -15^\circ$).

reduced molecular symmetry leads to the distribution of the nuclear potentials across 12 nuclear spheres. This distribution of charge across the larger number of scattering centers smears out the interference effect in THP. Similar behavior has been previously observed in (e,2e) TDCS that were attributed to Young-type interference effects.[30] Further, three body distorted waves calculations for small atoms (3DW) and molecules (M3DW) have also provided evidence to support the deep minima observed in (e,2e) cross sections measured in an out-of-plane symmetric geometry.[31] In order to fully assess the importance of the present observations, we must first consider the limitations of the M3DW calculation for predicting cross sections.

We begin by discussing the behavior in the binary region. Comparing the calculated TDCS to the experimental data, it becomes apparent that the M3DW calculation works better, in terms of reproducing the shape of the experimental cross section, for 1,4-dioxane than THP. The clues for this may lie in the momentum profiles presented in Fig. 5 of our previous paper.[15] The momentum profiles for THP and 1,4-dioxane can be separated into two distinct components. First, we have the p-character from the O(2*p*) contribution which gives rise to the momentum profile peak at $q \sim 1.2$ a.u. Second, we have the *s*-character arising from the coupling of the O(2*p*) with the σ-bonding carbon frame. This s-character gives rise to the maximum in the momentum profile at $q = 0$ a.u. The momentum profiles for THP and 1,4-dioxane reflect the enhanced interaction that the two O(2*p*) electrons create with the carbon frame in the HOMO of 1,4-dioxane. The nature of these interactions has significant ramifications in the M3DW

calculation. Here the highly symmetric *s*-orbital character is maintained through the orientation averaging, but the phase of the *p*-orbital is problematic and may lead to this contribution being cancelled out. The enhanced *s*-character in 1,4-dioxane may explain the better agreement observed for this target than that seen for THP.

The present results display similar characteristics to those observed in Ar $(3p)^{-1}$ experiments[32] performed under asymmetrical kinematics with $E_0 = 195$ eV, $E_b = 20$ eV, and $\theta_a = -5^\circ$, -10°, and -15° that nearly match those presented here. In that study the shape of the measured data was well reproduced by hybrid distorted wave plus R-matrix calculations (DWB2-RM) that are available for atomic targets. The DWB2-RM calculations use a multi-configuration expansion of the initial and final target states, but do not directly include post collision interaction (PCI) effects. The results from that study are interesting for two reasons. First, it suggests that the target description may hold the key to accurately reproducing the shape of the binary feature in the present measurements. The experimental data in the binary region for argon are quite asymmetric, being skewed with the maximum intensity at the larger scattering angles. This behavior is somewhat reproduced in argon by the DWB2-RM method, that provides a seemingly adequate description of the collision through the use of distorted waves for the incident and fast outgoing electron, and a coupling of a slow electron with an accurate target description. The key interaction to improve cross section calculations for molecules might therefore be an improved description of the coupling of the slow ejected electron to the target, and how it may change the target structure, that is neglected in the present study. Second, despite the aforementioned good shape agreement, under the more forward scattering condition of $\theta_a = -5^\circ$ or -10° the DWB2-RM calculations underestimated the shift of these experimental binary features from the momentum transfer direction to larger scattering angles. This is also apparent in our present measurements for THP and 1,4-dioxane, where the experimentally measured binary peak is substantially shifted away from the momentum transfer direction. The shift in the TDCS away from the momentum transfer direction is classically described as a PCI effect, which is not directly included in the DWB2-RM calculation. As such, the inclusion of PCI may still play an important role under these scattering conditions. This is in contrast to previous calculations on molecules[17] that were performed both with and without PCI effects, and displayed minimal difference. The quality of the slow-ejected electrons coupling with the target description may therefore influence the ability to fully assess any PCI effect.

As both THP and 1,4-dioxane have O($2p$) orbital contributions, the substantial experimental intensity seen in the 90°–120° angular regions, underestimated theoretically, may have similar origins to the skewed asymmetrical behavior observed in the binary peak of Ar $(3p)^{-1}$. In this respect, the ionization of orbitals with non-zero orbital angular momentum is known to be problematic in computing orientation averaged cross sections. The observed similarities between the experimental measurements of ionization dynamics with complex targets and those of atoms are encouraging, in particular, for trying to relate well-established atomic physics phenomena to molecular targets.

For both THP and 1,4 dioxane, the experimental measurements for scattering angles of $\theta_a = -10^\circ$, and -15° all exhibit substantial intensity in the recoil region. Here the observed intensities are comparable to that observed for other large molecules under very similar kinematical conditions, such as THFA.[17] Here we note that the M3DW calculations fail to reproduce the experimental intensity observed in the recoil region under all kinematical conditions.

To try and address these issues, work has begun on performing distorted wave calculations that perform a "proper" average over all molecular orientations studied in the experiment. The first calculations have been performed for CH_4 and the properly averaged results are in much better agreement with experiment.[33] It is hoped that, through such an averaging approach, the discrepancies observed between the theoretical calculations and experimental results can be resolved at least in part. However, the full averaging approach is computationally demanding and cannot be performed with available local computing resources. We performed the CH_4 calculation using our Extreme Science and Engineering Discovery Environment (XSEDE) allocation for this year and we will submit a proposal to examine other molecules next year.

The present study identifies a clear path forward for how some of the limitations encountered in dynamical (e,2e) investigations of molecular targets can be understood, through performing systematic evaluations of the approximations employed for atomic targets. This is an important prerequisite for developing reliable scattering models for electron-impact ionization of molecules. It is also essential for ascertaining if current predictions of interference effects, as displayed by the deep theoretical minima, are real. Further, dynamical (e,2e) experiments for molecular targets, that can achieve higher statistical precision over larger angular ranges, in the hope of observing these deep minima, are also desirable.

V. CONCLUSIONS

We have presented experimental measurements and theoretical calculations for triple differential cross sections of the electron impact ionization of the HOMO's of THP and 1,4-dioxane under asymmetrical kinematical conditions. The data for all electron scattering angles exhibit relatively large recoil peaks, which were underestimated by the M3DW calculations. The binary peaks calculated at the M3DW level resemble those observed experimentally at all scattering angles. Earlier measurements for Ar $(3p)^{-1}$, under similar experimental conditions, give results which suggest that the target description in the calculation may be inadequate in this kinematic regime. Specifically, this result may reflect the inadequate description of *p*-like orbital contributions in the spherically averaged Dyson orbital. In spite of these short comings, the M3DW suggests that interference phenomena relating to the structure of the target may be reflected in the TDCS. The suggestion of interference effects in the theoretical cross sections thus provides significant opportunities to glean more insights into the dynamics of ionization from complex targets. Finally, work has begun at calculating cross sections within

the 3-distorted wave framework that perform a proper average over all molecular orientations studied in the experiment and first results are encouraging.

ACKNOWLEDGMENTS

This research was supported by the Australian Research Council (ARC) Centre of Excellence for Antimatter-Matter Studies and by the US National Science Foundation under Grant No. PHY-1068237 (H.C. and D.H.M.). G.B.S. thanks CAPES (Proc. No. BEX 17756/12-0) and Flinders University for financial assistance during his stay in Australia. D.B.J. gratefully acknowledges support provided through an ARC Discovery Early Career Researcher Award.

[1]L. Sanche, in *Radiation Induced Molecular Phenomena in Nucleic Acids*, edited by M. Shukla and J. Leszczynski (Springer, Netherlands, 2008), Vol. 5, p. 531.
[2]B. Boudaiffa, P. Cloutier, D. Hunting, M. A. Huels, and L. Sanche, Science **287**, 1658 (2000).
[3]S. M. Pimblott and J. A. LaVerne, Radiat. Phys. Chem. **76**, 1244 (2007).
[4]A. G. Sanz, M. C. Fuss, A. Munoz, F. Blanco, P. Limao-Vieira, M. J. Brunger, S. J. Buckman, and G. Garcia, Int. J. Radiat. Biol. **88**, 71 (2012).
[5]Z. L. Petrović, S. Marjanović, S. Dujko, A. Banković, G. Malović, S. Buckman, G. Garcia, R. White, and M. Brunger, Appl. Radiat. Isot. **83**(Part B), 148 (2014).
[6]Z. Francis, S. Incerti, R. Capra, B. Mascialino, G. Montarou, V. Stepan, and C. Villagrasa, Appl. Radiat. Isot. **69**, 220 (2011).
[7]I. Plante and F. A. Cucinotta, New J. Phys. **10**, 125020 (2008).
[8]S. Agostinelli *et al.*, Nucl. Instrum. Methods Phys. Res., Sect. A **506**, 250 (2003).
[9]J. Allison *et al.*, IEEE Trans. Nucl. Sci. **53**, 270 (2006).
[10]F. Salvat, J. M. Fernandez-Varea, and J. Sempau, *PENELOPE2011, A Code System for Monte-Carlo Simulation of Electron and Photon Transport* (OECD - Nuclear Energy Agency, 2011).
[11]C. Champion, C. Le Loirec, and B. Stosic, Int. J. Radiat. Biol. **88**, 54 (2012).
[12]D. S. Milne-Brownlie, S. J. Cavanagh, B. Lohmann, C. Champion, P. A. Hervieux, and J. Hanssen, Phys. Rev. A **69**, 032701 (2004).
[13]J. Builth-Williams, S. M. Bellm, D. B. Jones, H. Chaluvadi, D. Madison, C. G. Ning, B. Lohmann, and M. J. Brunger, J. Chem. Phys. **136**, 024304 (2012).
[14]S. M. Bellm, C. J. Colyer, B. Lohmann, and C. Champion, Phys. Rev. A **85**, 022710 (2012).
[15]J. D. Builth-Williams *et al.*, J. Chem. Phys. **139**, 034306 (2013).
[16]D. B. Jones *et al.*, Chem. Phys. Lett. **572**, 32 (2013).
[17]S. M. Bellm *et al.*, J. Chem. Phys. **136**, 244301 (2012).
[18]S. J. Cavanagh and B. Lohmann, J. Phys. B: At. Mol. Opt. Phys. **32**, L261 (1999).
[19]C. J. Colyer, S. M. Bellm, B. Lohmann, G. F. Hanne, O. Al-Hagan, D. H. Madison, and C. G. Ning, J. Chem. Phys. **133**, 124302 (2010).
[20]M. Yamauchi, H. Yamakado, and K. Ohno, J. Phys. Chem. A **101**, 6184 (1997).
[21]C. Lee, W. Yang, and R. G. Parr, Phys. Rev. B **37**, 785 (1988).
[22]C. Fonseca Guerra, J. G. Snijders, G. te Velde, and E. J. Baerends, Theor. Chem. Acc. **99**, 391 (1998).
[23]S. J. Ward and J. H. Macek, Phys. Rev. A **49**, 1049 (1994).
[24]J. B. Furness and I. E. McCarthy, J. Phys. B: At. Mol. Phys. **6**, 2280 (1973).
[25]J. P. Perdew and A. Zunger, Phys. Rev. B **23**, 5048 (1981).
[26]N. T. Padial and D. W. Norcross, Phys. Rev. A **29**, 1742 (1984).
[27]J. F. Gao, D. H. Madison, and J. L. Peacher, J. Chem. Phys. **123**, 204314 (2005).
[28]J. F. Gao, J. L. Peacher, and D. H. Madison, J. Chem. Phys. **123**, 204302 (2005).
[29]J. F. Gao, D. H. Madison, and J. L. Peacher, J. Phys. B: At. Mol. Opt. Phys. **39**, 1275 (2006).
[30]D. S. Milne-Brownlie, M. Foster, J. Gao, B. Lohmann, and D. H. Madison, Phys. Rev. Lett. **96**, 233201 (2006).
[31]J. Colgan, O. Al-Hagan, D. H. Madison, A. J. Murray, and M. S. Pindzola, J. Phys. B: At. Mol. Opt. Phys. **42**, 171001 (2009).
[32]X. Ren, A. Senftleben, T. Pflüger, A. Dorn, K. Bartschat, and J. Ullrich, Phys. Rev. A **83**, 052714 (2011).
[33]H. Chaluvadi, C. G. Ning, and D. H. Madison, "Theoretical triple differential cross sections of methane molecule by proper averaged method," Phys. Rev. A (submitted).